Measurements and Signal Processing for Distributed Sensing with Centimeter-Scale Spatial Resolution by BOFDA

Bibekananda Sahoo [1], Abhipsa Sahoo [2], Jugajyoti Sahu [3], Jagamohan Moharana [4], Nilachal Patra [5]
SANTOSH KUMAR JHA[6]
[1, 2, 3, 4, 5] Gandhi Institute for Education & Technology, Baniatangi, Khordha, Odisha
[6]NM Institute of Engineering & Technology,Bhubaneswar,Odisha

bibekanandasahoo@giet.edu.in, abhipsasahoo@giet.edu.in, jugajyotisahu@giet.edu.in, jagamohanmoharana@giet.edu.in, nilachalpatra@giet.edu.in

Abstract: *In this study, we combine Brillouin optical frequency-domain analysis (BOFDA) and signal processing to exhibit high spatial (_3 cm) and spectral (_30 MHz) resolution Brillouin sensing. To remove erroneous effects related to acoustic wave modulation and important in the high spatial resolution regime from the obtained data, an iterative technique is used. The suggested approach can reconstruct the Brillouin shift profile with the maximum spatial resolution permitted by the system bandwidth, according to experimental experiments.*

Index Terms: Optical fiber sensors, strain measurement, temperature measurement.

1. Introduction

Distributed fiber sensors based on stimulated Brillouin scattering (SBS) have been studied for over two decades, and several schemes have been developed in the form of reflectometry or analysis for the measurement of local Brillouin frequency u_B . Time-domain approach has several benefits, among which a straightforward interpretation of the retrieved traces, as any time instant on the acquired trace corresponds to a well-defined position along the fiber through the time-of-flight of the pulse. However, the time-domain scheme suffers from a fundamental limitation related to the time required for the acoustic field to be excited by the interacting pump pulse. For a pump pulse width of 10 ns (corresponding to a spatial resolution 1 m) or lower, the amplification of the Stokes beam obeys to a broadened and weaker gain spectral curve [1], [2]. This results in a low signal-to-noise *S=N* ratio and low accuracy in the retrieval of u_B . Different approaches have been proposed to overcome this limitation. The more relevant are those based on 1) dark pulses [3]; 2) differential pulse-width pairs with or without phase shift [4], [5]; and 3) dynamic Brillouin gratings [6]. By these methods centimeter- or even millimeter-scale spatial resolution has been demonstrated.

All the mentioned techniques operate in the time-domain, i.e., rely on some form of pulsing of the pump beam. Beside these approaches, a correlation-based technique has been developed to enhance spatial resolution down to 1 cm [7]. However, the periodicity of the synthesized correlation function imposes a limit on the maximum number of sensing points [8]. As an alternative, the Brillouin optical frequency-domain analysis (BOFDA) is applicable to obtain spatial resolution in

Brillouin-based distributed sensors [9], [10]. The pump beam in BOFDA systems is not pulsed; rather its intensity is sinusoidally modulated. A baseband transfer function is acquired by recording the amplitude and phase of the modulation induced by SBS on the Stokes beam intensity, over a range of modulation frequencies. The main advantage of the method stems from the fact that Stokes and pump optical carriers preactivate a stationary acoustic wave, thanks to which the corresponding Brillouin gain curve keeps its natural linewidth (30 MHz in standard silica fibers). As a result, u_B can be determined with high accuracy even if operating in the high-spatial resolution regime [11]. This effect is somewhat similar to the one observed in the dark-pulse method, in which a stationary (narrowband) acoustic wave, preactivated by the pump dc component, leads to high spectral resolution [3].

On the other hand, it has been also shown that the interaction between the pump beam and the modulated component of the acoustic field has a detrimental effect on the accuracy of the mea- surements in BOFDA schemes [11], as it produces artifacts in the retrieved Brillouin gain spectra (BGSs) when a nonuniform u_B profile is present along the fiber. A similar limitation is found in systems making use of a pulsed pump with a baseline [12], in which the decaying acoustic field excited by pulse passage continues to interact with the pump baseline, creating artifacts in the detected Stokes signal.

In this paper, we demonstrate that applying a iterative correction algorithm to the acquired BOFDA measurements it is possible to minimize the effects related to acoustic field sidebands, removing resolution degrading features. Experimental results at 29 mm spatial resolution are reported in the following.

2. Description of the Algorithm

In BOFDA schemes a CW probe wave and a counterpropagating, intensity-modulated pump wave interact along the fiber. The probe wave is phase- and amplitude-modulated while it propagates down the fiber due to SBS interaction with the pump, provided that the frequency shift between the two beams falls below the BGS. By scanning the modulation frequency of the pump wave, a complex baseband transfer function is acquired for each fixed pump-probe frequency shift. In a small signal approximation, the transfer function can be expressed as [11]

$$TF(\omega_m) = \frac{I_{S1}(\omega_m)}{I_{p1}(\omega_m)} = \int_0^L E_{s0}(z)\, g_{B;ac}(z;\omega_m)\, e^{-2j\omega_m n z/c}\, dz. \quad (1)$$

where ω_m is the modulation frequency, I_{S1} and I_{p1} are the complex ac intensity components of the transmitted probe signal and launched pump signal, respectively, E_{s0} is the stationary probe field, L is the fiber length, n is the fiber refractive index, c is the light velocity in the vacuum, z is the distance along the fiber axis from the input section of the modulated pump, and $g_{B;ac}$ is the ac Brillouin gain given by

$$g_{B\,ac}(z;\omega_m) = \frac{g_{B0}}{2}\left[\frac{1}{1-j\frac{\Omega(z)}{\Gamma_1}} + \frac{1}{1+j\frac{\Omega(z)}{\Gamma_1}} + \frac{1}{1-j\frac{\Omega(z)-\omega_m}{\Gamma_1}} + \frac{1}{1+j\frac{\Omega(z)+\omega_m}{\Gamma_1}}\right]. \quad (2)$$

In (2), g_{B0} is the SBS peak gain coefficient, Γ_1 is the acoustic damping rate, and $\Omega(z) = 2\pi(\nu_p - \nu_B(z))$ is the z-dependent detuning, i.e., the difference between the pump- probe frequency shift and the local u_B. As discussed in [11], the first two terms in the rhs of (2) describe the interaction between the acoustic wave carrier and the pump wave sidebands. These terms are essential for obtaining spatial resolution in distributed sensing. On the other hand, the last two terms on the right-hand side of (2) describe the interaction between the pump wave carrier and the acoustic sidebands, and are responsible for the appearance of "ghost" peaks in the BGSs in case of nonuniform distribution of u_B.

In standard BOFDA, the acquired transfer functions are inverse Fourier transformed in order to achieve positional information, while a peak-searching algorithm is applied to the transformed data

in order to extract the ν_B profile. In our method, the same procedure is applied to obtain a first estimation of the ν_B profile. Due to the influence of acoustic wave sidebands, the estimated ν_B profile will be affected by systematic errors, in a measure depending on the spectral content of the ν_B distribution. In order to obtain a more accurate reconstruction, the retrieved profile may be used to estimate the distorting component affecting the frequency-domain data by use of the following relations:

$$TF^{dist,1}(\omega_m) = E_{s0}(L)\int_0^L E^1_{s0}(z)\, g_B^{dist,1}(z;\omega_m)\, e^{-2j\omega_m n/c}\, dz \quad (3)$$

with $g_B^{dist,1}(z;\omega_m)$ given by

$$g_B^{dist,1}(z;\omega_m) = \frac{g_{B0}}{2}\left(\frac{1}{1-j\frac{\Omega^1(z)-\omega_m}{\Gamma_1}} + \frac{1}{1+j\frac{\Omega^1(z)+\omega_m}{\Gamma_1}}\right). \quad (4)$$

In (3) and (4), $E^1_{s0}(z)$ is the stationary component of the Stokes field, as computed by solving the steady-state SBS equations by using the initial estimate of the Brillouin frequency shift profile $\nu_{B0}(z)$ [13], while $\Omega^1(z) = 2\pi(\Delta\nu_{pp} - \nu_{B0}(z))$. The calculations expressed by (3) and (4) must be done separately for each pump-probe frequency shift used for the measurements. The distorting term expressed by (3) is then subtracted from each acquired transfer function, so as to obtain a corrected transfer function for each pump-probe frequency shift. The peak-searching algorithm is then applied to the inverse Fourier transform of the corrected data, in order to retrieve a new reconstruction of the Brillouin shift profile. We note that, as the ν_{B0} profile employed to calculate the distorting terms is generally affected by systematic errors, the calculation expressed by (3) and (4) is only approxi- mated at this first step. On the other hand, the described procedure can be iterated a suitable number of times, until a convergence condition is reached. At the end of each cycle, a new reconstruction of the Brillouin shift profile is available, which in turns can be employed to perform a more accurate correction of the transfer functions. The stop criterion can be defined on the basis of the norm of the difference between two successive estimations of the Brillouin shift profile. In the experimental results reported below, a minimum standard deviation of 1 MHz was adopted as the threshold condition.

By applying the proposed algorithm, the artifacts appearing in the acquired BGS in case of a nonuniform ν_B profile are progressively filtered out by subtraction of the distorting term from the raw data. By removing the degrading features screening the real Brillouin response of the system, a more accurate reconstruction of the ν_B profile is achieved, as demonstrated by the experimental tests described in the next section.

3. Experimental Results

The BOFDA experimental configuration employed to validate the proposed method is depicted in Fig. 1. A 1551-nm 40-mW distributed-feedback laser diode was used as the light source. The polarized output of the laser diode was split into two distinct channels to allow both the pump and signal waves to be derived from the same optical source. The signal was generated in the upper channel, where an integrated electrooptic intensity modulator (IM1) driven by a radio frequency synthesizer in a suppressed carrier configuration, creates sidebands, one of which (the upper one) is filtered out by a narrowband (10 GHz) fiber Bragg grating filter.

In the lower channel, a second electrooptic intensity modulator (IM2) driven by the RF output of a vector network analyzer, was used to modulate the pump beam across the range of frequencies chosen for the measurement of the transfer functions. Both pump and signal waves were amplified before being injected in the sensing fiber. A polarization scrambler (PS) was employed to minimize the gain fluctuations due to changes in the state of polarization of the pump along the sensing fiber. A wideband (3.5-GHz) photodetector with a transimpedance gain of 1.100 V/W was used to convert the received optical signal in an RF signal, which was then demodulated by the network analyzer.

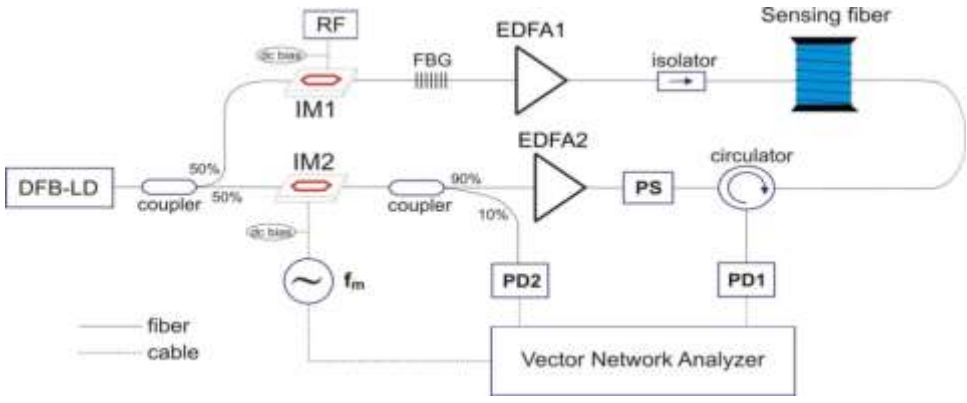

Fig. 1. Experimental setup for BOFDA measurements. DFB-LD: diode laser. FBG: fiber Bragg grating. EDFA: erbium-doped fiber amplifier. PS: polarization scrambler. IM: intensity modulator. PD: photodetector.

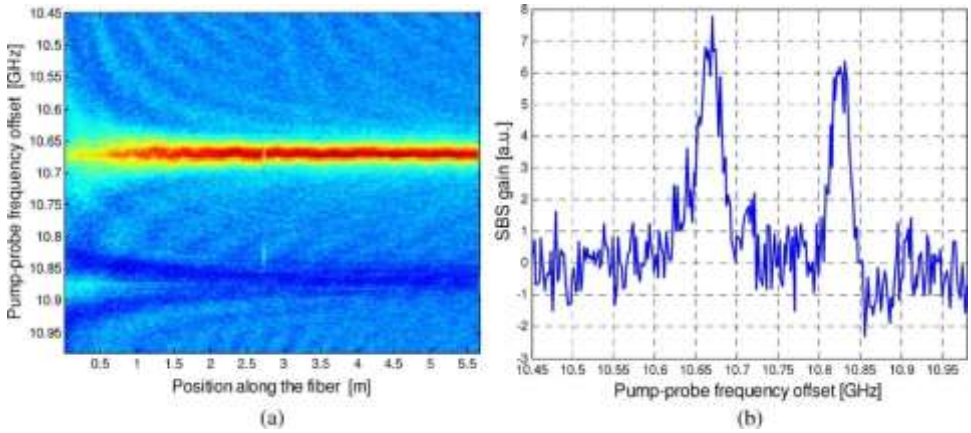

Fig. 2. (a) BGS distribution along a 5.5-m fiber strand with a 3-cm spot located in the middle, as obtained by applying an inverse Fourier transform to the acquired data. (b) BGS acquired at the perturbation section ðz ¼ 2:72 mÞ.

The latter operates from 3 kHz to 4.5 GHz, corresponding to a maximum sensing range and a minimum spatial resolution equal to 30 km and 22 mm, respectively [9]. In our experiments, the transfer functions were acquired up to 3.5 GHz (29 mm spatial resolution) due to limit imposed by the photodetector bandwidth. Also, the network analyzer was set to operate with an intermediate frequency (IF) bandwidth of 10 kHz and a number of averages equal to 10.

As a first example, we prepared a test fiber by fusion splicing a 3-cm segment of fiber B u_B 10 825 MHz ðbetween two strands of fiber A u_B 10 668 MHz . Both fibers were single- mode optical fibers (SMF) but were produced by different manufacturers. The overall length of the sensing fiber was 5.5 m. The measurement was performed by setting the output powers from EDFA1 and EDFA2 to 1.5 dBm and 17 dBm, respectively. We first show in Fig. 2(a) the BGS distribution obtained by inverse Fourier transforming the transfer functions acquired for a range of microwave frequencies ranging from 10 450 MHz to 10 980 MHz at a 2-MHz step. While the 3-cm perturbation is visible in the middle of the plot, a quantitative estimation of the Brillouin frequency shift profile requires a Lorentzian fitting procedure to be applied to each BGS. Actually, the capability of the sensor to spatially resolve a narrow spot should be evaluated on the basis of the spectral purity of the BGS at the perturbed section [14].

We report in Fig. 2(b) the BGS at the perturbation z 2:72 m as obtained by performing a vertical cut to the image shown in Fig. 2(a). Although the correct peak centered at

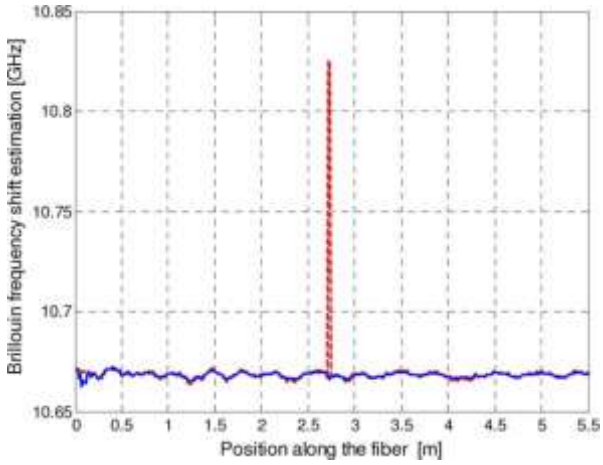

Fig. 3. Brillouin frequency shift profile estimation obtained by peak-searching the rough data (solid blue curve) or the corrected data (dashed red curve).

ν_{pp} 10.825 MHz is detected, a spurious peak at the unperturbed Brillouin shift ν_{pp} 10.668 MHz is also present. As discussed in [11], the spurious peak arises from interaction of the modulated component of the acoustic wave and the pump wave when their frequency shift is around the unperturbed ν_B. When fitting the BGS shown in Fig. 2(b) with a single Lorentzian curve, the correct value of the local ν_B cannot be detected unambiguously. The method described in the previous section has therefore been applied to the acquired data. At first, an initial estimate of the Brillouin shift profile was carried out by peak-searching the spectra shown in Fig. 2(a). The result is shown in Fig. 3 (solid blue line). It is seen that the central perturbation is not detected by the fitting procedure, due to the fact that the spurious peak in Fig. 2(b) is higher than the correct peak. Nonetheless, the obtained profile was employed to perform the calculation of the distorting terms affecting the acquired data, as expressed by (3) and (4), and therefore to correct the data. The corrected data were employed to produce a new ν_B profile, which was then compared to the initial guess profile. The above procedure was repeated until the norm of the difference between two successive ν_B reconstruction was found to be less than 1 MHz. In this test, the convergence condition was reached after five iterations. Note that the time consumed for each iteration was only a few tens of seconds on an Intel i7 processor running under MATLAB environment.

In Fig. 3, we report the ν_B reconstruction obtained by the proposed iterative method. In this case, the central perturbation is correctly retrieved. The effectiveness of the method can be also appreciated by showing the inverse Fourier transform of the corrected data [see Fig. 4(a)], as well as the corresponding vertical cut at the perturbation section [see Fig. 4(b)]. Comparing Figs. 2(b) and 4(b), a high suppression of the spurious peak in the perturbed BGS can be seen, allowing an unambiguous estimation of the local Brillouin frequency shift. It is also important to note that the spectra acquired are narrowband (27 MHz) along the whole fiber, as typical for BOFDA systems [11].

As next test case, we constructed a 8.5-m SMF sample consisting of nine cascaded fiber portions of type A, or type C ν_B 10.715 MHz . The four perturbations had a length of 20 cm, 10 cm, 10 cm, and 3 cm [see Fig. 5(a)]. In Fig. 5(b), we report the inverse Fourier transform of the acquired data. Similarly to the previous case, we observe a nonnull Brillouin gain at resonance of fiber A in correspondence of the four perturbations. Also, a progressive decrease of the Brillouin gain along the fiber sample is observed, due to the splice loss at each fiber A–fiber C junction.

The proposed method was then applied to the raw data shown in Fig. 5(b). The inverse Fourier transforms of the corrected data obtained at the end of the iterative process are shown in Fig. 5(c). For this test case, the convergence condition was reached after six iterations. To illustrate the benefits provided by the proposed method, we report in Fig. 6 the Brillouin shift profile ν_{B0} obtained by processing the raw data (solid blue line), compared to the Brillouin shift profile obtained by

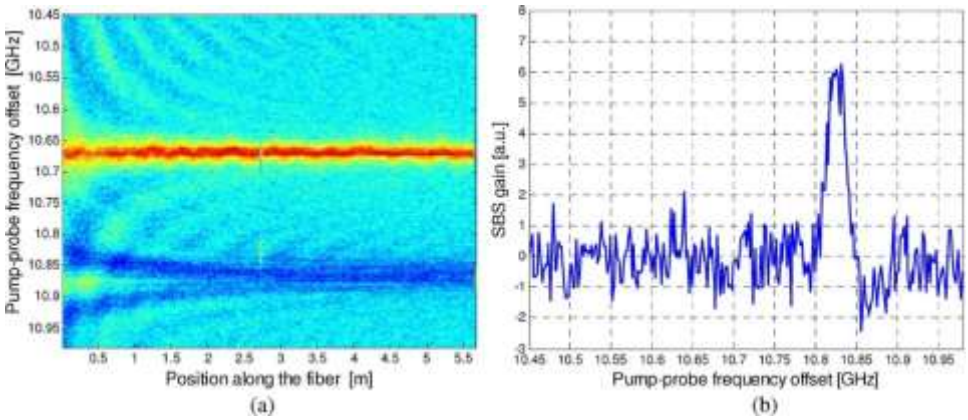

Fig. 4. (a) BGS distribution along a 5.5-m fiber strand with a 3-cm spot located in the middle, as obtained by applying the proposed method. (b) BGS at the perturbation section z 2:72 m as obtained by applying the proposed method.

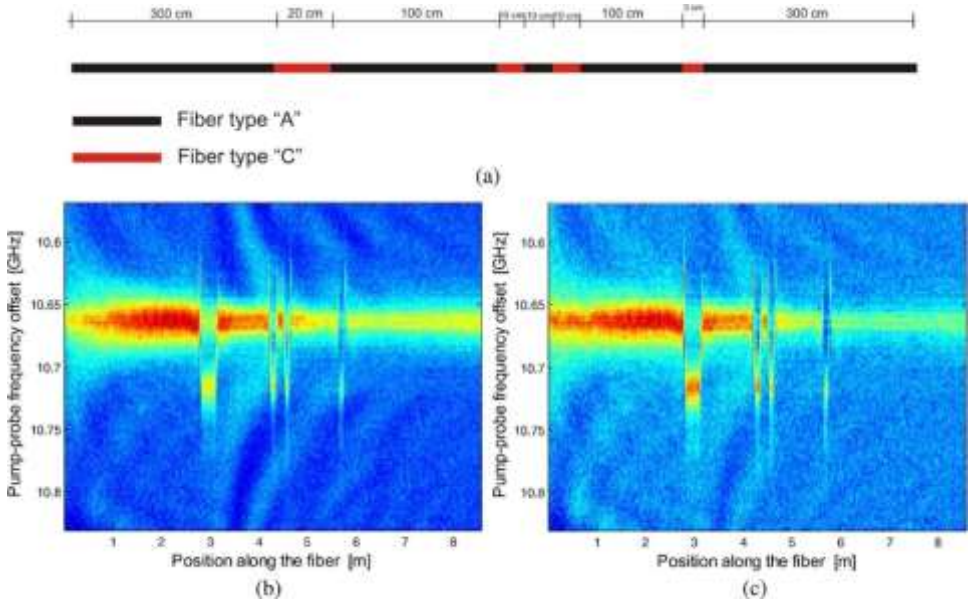

Fig. 5. (a) SMF sample comprising nine cascaded fiber portions. (b) BGS distribution along the prepared SMF sample, as obtained by applying an inverse Fourier transform to the acquired data and (c) after application of the proposed method.

processing the corrected data (dashed red line). Note that the Brillouin shift at the perturbations was underestimated in the initial guess reconstruction, especially in the first, wider spot. As discussed before, these errors are due to the failing of the fitting procedure when the latter is applied to a double-peaked spectral shape. On the other hand, applying the correction algorithm leads to a suppression of the spurious peaks in the spectra, resulting in a more accurate reconstruction of the Brillouin frequency shift profile.

It is also useful to compare the original measured BGS and the corrected BGS at two significant sections of the fiber: In particular, Fig. 7(a) refers to section z 2:95 m, i.e., in the middle of the first, wider spot, while Fig. 7(b) refers to section z 4:65 m, at which an undershoot of the Brillouin frequency shift is observed in the processed data. Note that the revealed undershoot should be attributed to the compressive strain locally induced by the shrinking of the 60 mm-long protection sleeve at the splice joint.

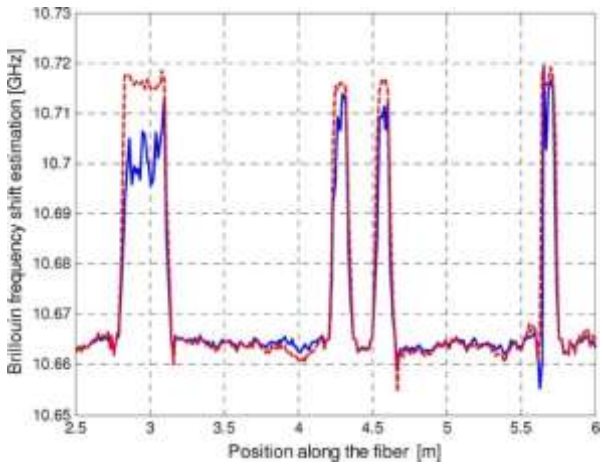

Fig. 6. Brillouin frequency shift profile estimation obtained by processing the raw data (solid blue curve) or the corrected data (dashed red curve).

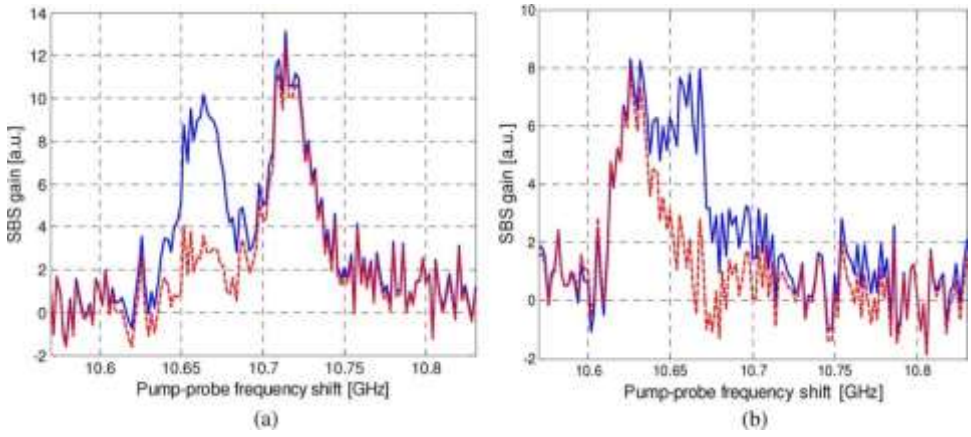

Fig. 7. Acquired BGS (solid blue curve) and corrected BGS (dashed red curve) at (a) z ¼ 2:95 m and (b) z ¼ 4:65 m, relative to the fiber sample shown in Fig. 5(a).

As a final example, we chose to test the validity of the proposed algorithm in the case of a gradually changing Brillouin shift frequency profile. To this aim, a portion of a 11 m-long fiber was attached, by use of a cyanoacrylate adhesive, along the top surface of an L-shaped, 3.7-m long cantilever aluminum beam with equal legs of 3 cm. Details on the geometry of the beam and fiber installation procedure can be found in [15]. After fiber installation, a first measurement of Brillouin shift profile was acquired as reference profile, in order to take into account the bonding-induced strains. Then, two measurements were performed by imposing a vertical displacement to the free end of the cantilever downward or upward to induce tensile strains or compressive strains along the attached fiber.

We report in Fig. 8 the results of these measurements, as obtained by directly processing the acquired data or by using the proposed iterative method (six iterations).

In the latter case, both Brillouin shift profile with the bent cantilever and reference profile were separately reconstructed according to the proposed method, and then subtracted to retrieve the strain distribution shown in Fig. 8. It is seen that the standard reconstruction technique fails to detect accurately the strain profile, even though the nominal spatial resolution of the sensor (29 mm) is well below the cantilever length. On the other hand, the proposed method provides more accurate results, as verified by comparison with the theoretical profiles also shown in Fig. 8. In particular, the

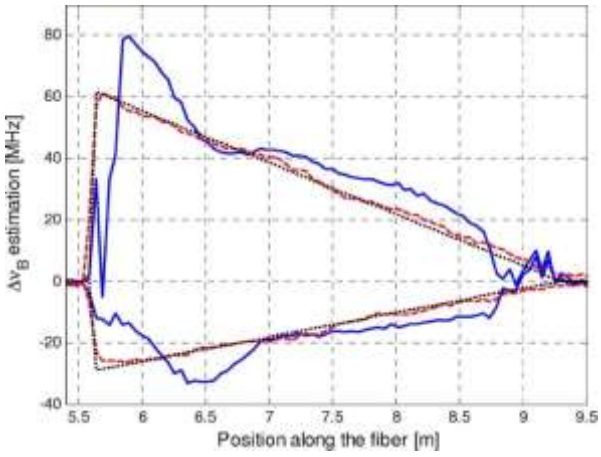

Fig. 8. Estimation of the Brillouin shift changes along a 3.7-m-long cantilever beam, obtained by processing the rough data (solid blue curves) or the corrected data (dashed red curves). The graph also shows the theoretical profiles (dotted black curves). The fiber portion attached to the beam is comprised of between *z* 5:5 m to *z* 9:2 m. Also, no effort was made in order to have a maximum applied tensile strain equal to the maximum applied compressive strain.

standard deviation between the theoretical profile and the classical reconstruction was =7.2 MHz for the tensile (positive) strain profile and =3.9 MHz for the compressive (negative) strain profile, whereas the corresponding values in case of iterative reconstruction were =1.8 MHz for the tensile strain profile and = 0.9 MHz for the compressive strain profile.

4. Conclusion

Distributed sensing at 29-mm spatial resolution was experimentally demonstrated by use of BOFDA and signal processing. The proposed signal processing method permits to remove degrading features in the retrieved spectra, allowing to reach full spatial resolution.

When compared to BOTDA method, BOFDA technique takes advantage of a simpler descriptive model of the SBS interaction, as scattering is excited by a single pump modulation frequency at a time, rather than by a wave packet as in case of a pulsed pump. A simple model description permits to identify and efficiently compensate degrading features in the acquired data, as well as to develop new measuring schemes to improve performances. We must note that recently, a post-processing method for time-domain schemes have been proposed, aimed to compensate the interfering effects associated with acoustic wave relaxation [16]. Although the method presented in [16] is not iterative, and thus potentially faster than the one proposed in this paper, it requires a deconvolution of the acquired data, which generally leads to a deterioration of the *S=N* ratio. Also, the method proposed in [16] to correct the acquired data only tries to recover the original response in the resonance case, while off-resonance oscillations of the acoustic wave are not taken into account.

Nevertheless, BOFDA method also presents some drawbacks with respect to BOTDA: the maximum sensing length may be generally limited by pump depletion, resulting from the interaction between the pump and signal optical carriers along the whole fiber length. Pump depletion can be reduced by employing a sufficiently weak probe signal, or it can be compensated by injecting both Stokes and anti-Stokes waves at the *z L* input [17], [18]. By this technique, BOFDA measure- ments up to 5 km have been demonstrated [17].

Another important aspect is the acquisition time of BOFDA method, especially when long sensing range and high spatial resolution are simultaneously required. Actually, the number of sampling points to be acquired for each transfer function (and therefore the acquisition time) increases linearly with the ratio between fiber length and spatial resolution [9], while being virtually indepen- dent of the fiber length in time-domain schemes. In our experimental tests, involving fiber lengths of a few meters. The overall acquisition

time was about 1 min. Therefore, for a fiber length of 1 km the

acquisition time would increase up to a few hours if keeping the same spatial resolution. Note, however, that in our system most of the measuring time was due to data transfer from the network analyzer to the PC, realized by a LAN connection. A faster data transfer protocol would permit to reduce the overall acquisition time. As processing time is concerned, we note that processing requires an inverse Fourier transform to be performed on the acquired and corrected data: Algorithms for fast computation of Fourier transforms can be efficiently implemented, e.g., by digital signal processors.

References

[1] A. Fellay, L. Thévenaz, M. Facchini, M. Niklès, and P. A. Robert, BDistributed sensing using stimulated Brillouin scattering: Towards ultimate resolution,[in *Proc. 12th Int. Conf. Opt. Fiber Sens. Tech. Dig.*, 1997, pp. 324–327.
[2] H. Naruse and M. Tateda, BTrade-off between the spatial and the frequency resolutions in measuring the power spectrum of the Brillouin backscattered light in an optical fiber,[*Appl. Opt.*, vol. 38, no. 31, pp. 6516–6521, Nov. 1999.
[3] A. W. Brown, B. G. Colpitts, and K. Brown, BDark-pulse Brillouin optical time-domain sensor with 20-mm spatial resolution,[*J. Lightwave Technol.*, vol. 25, no. 1, pp. 381–386, Jan. 2007, DOI:10.1109/JLT.2006.886672.
[4] W. Li, X. Bao, Y. Li, and L. Chen, BDifferential pulse-width pair BOTDA for high spatial resolution sensing,[*Opt. Exp.*, vol. 16, no. 26, pp. 21 616–21 625, Dec. 2008.
[5] S. M. Foaleng, M. Tur, J.-C. Beugnot, and L. Thévenaz, BHigh spatial and spectral resolution Long-range sensing using Brillouin echoes,[*J. Lightwave Technol.*, vol. 28, no. 20, pp. 2993–3003, Oct. 2010, DOI: 10.1109/JLT.2010.2073443.
[6] K. Y. Song, W. Zou, Z. He, and K. Hotate, BOptical time-domain measurement of Brillouin dynamic grating spectrum in a polarization-maintaining fiber,[*Opt. Lett.*, vol. 34, no. 9, pp. 1381–1383, May 2009.
[7] K. Hotate and M. Tanaka, BDistributed fiber Brillouin strain sensing with 1-cm spatial resolution by correlation-based continuous-wave technique,[*IEEE Photon. Technol. Lett.*, vol. 14, no. 2, pp. 179–181, Feb. 2002.
[8] L. Thévenaz, BInelastic scatterings and application to distributed sensing,[in *Advanced Fiber Optics∀Concepts and Technology*, L. Thévenaz, Ed. Lausanne, Switzerland: EPFL Press, 2011.
[9] D. Garus, K. Krebber, F. Schliep, and T. Gogolla, BDistributed sensing technique based on Brillouin optical-fiber frequency-domain analysis,[*Opt. Lett.*, vol. 21, no. 17, pp. 1402–1404, Sep. 1996.
[10] R. Bernini, A. Minardo, and L. Zeni, BStimulated Brillouin scattering frequency-domain analysis in a single-mode optical fiber for distributed sensing,[*Opt. Lett.*, vol. 29, no. 17, pp. 1977–1979, Sep. 2004.
[11] A. Minardo, G. Testa, L. Zeni, and R. Bernini, BTheoretical and experimental analysis of Brillouin scattering in single- mode optical fiber excited by an intensity- and phase-modulated pump,[*J. Lightwave Technol.*, vol. 28, no. 2, pp. 193–200, Jan. 2010.
[12] V. P. Kalosha, E. Ponomarev, L. Chen, and X. Bao, BHow to obtain high spectral resolution of SBS-based distributed sensing by using nanosecond pulses,[*Opt. Express*, vol. 14, no. 6, pp. 2071–2078, Mar. 2006.
[13] G. P. Agrawal, *Nonlinear Fiber Optics,* 4th ed. New York: Academic, 2007.
[14] A. Minardo, R. Bernini, and L. Zeni, BNumerical analysis of single pulse and differential pulse-width pair BOTDA systems in the high spatial resolution regime,[*Opt. Exp.*, vol. 19, no. 20, pp. 19 233–19 244, Sep. 2011.
[15] R. Bernini, A. Minardo, G. Testa, and L. Zeni, BDynamic strain measurements on a cantilever beam using stimulated Brillouin scattering,[*Smart Mater. Struct.*, vol. 19, no. 4, p. 045024, Apr. 2010.
[16] J.-C. Beugnot, M. Tur, S. F. Mafang, and L. Thévenaz, BDistributed Brillouin sensing with sub-meter spatial resolution: Modeling and processing,[*Opt. Exp.*, vol. 19, no. 8, pp. 7381–7397, Apr. 2011.
[17] A. Minardo, R. Bernini, and L. Zeni, BA simple technique for reducing pump depletion in long-range distributed Brillouin fiber sensors,[*IEEE Sens. J.*, vol. 9, no. 6, pp. 633–634, Jun. 2009.
[18] A. Minardo, R. Bernini, and L. Zeni, BExtension of the maximum measuring range in distributed Brillouin fiber sensors by tuning the Stokes/anti-Stokes power ratio,[in *Proc. SPIE*, 2010, vol. 7653, pp. 76 533D-1–76 533D-3.